Articles

Structural Comparison of Five-Coordinate Thiolate-Ligated M^{II} = Fe^{II}, Co^{II}, Ni^{II}, and Zn^{II} Ions Wrapped in a Chiral Helical Ligand

Steven C. Shoner, Andrew M. Nienstedt, Jeffrey J. Ellison, Irene Y. Kung, David Barnhart, and Julie A. Kovacs*

Department of Chemistry, University of Washington, Seattle, Washington 98195

Received July 27, 1998

The syntheses and structures of two analogous five-coordinate mixed nitrogen/thiolate-ligated Co^{2+} and Fe^{2+} complexes are described and compared to their previously reported Zn^{2+} and Ni^{2+} analogues. The linear, single-chain $[S_2^{R2}N_3(Pr,Pr)]^{2-}$ (R = H, Me) ligands examined in this study wrap themselves around metal ions in both a clockwise and counterclockwise manner to afford a racemic mixture of chiral, helical molecules. $[Fe^{II}S_2N_3(Pr,Pr)]$ (**1**) crystallizes in the monoclinic space group $P2_1/c$ with $a = 7.853(2)$ Å, $b = 8.667(2)$ Å, $c = 26.079(5)$ Å, $\beta = 90.37(3)°$, $V = 1775.0(7)$ Å^3, and $Z = 4$. $[Co^{II}S_2^{Me2}N_3(Pr,Pr)]$ (**2**) crystallizes in the monoclinic space group $P2_1/c$ with $a = 9.389(2)$ Å, $b = 19.706(3)$ Å, $c = 12.165(2)$ Å, $\beta = 103.67(2)°$, $V = 2186(1)$ Å^3, and $Z = 4$. Trends in helicity and angular distortions in the Fe^{2+}, Co^{2+}, Ni^{2+}, Zn^{2+} series which correlate with ionic radius are described. It is suggested that ligand constraints are responsible for the increasing distortion observed (Fe ∼ Zn < Co ≪ Ni) in these structures and that similar constraints may alter the geometries of metalloenzyme active sites.

Introduction

One of the challenges to modeling the reactivity of cysteine-ligated metalloenzyme active sites,[1] the majority of which contain labile first-row metal ions, is that the requisite vacant or labile substrate binding sites are usually rendered inaccessible via the formation of thiolate-bridged dimers or oligomers.[2,3] Because heteroleptic multidentate ligands which mimic the mixed donor (e.g., N/S/O) environment found in many metalloenzymes[1] are not commercially available, ligand design and synthesis play a significant role in the synthetic modeling of these sites. Metal-templated Schiff base reactions provide a convenient method for the synthesis of multidentate thiolate/nitrogen ligands. The resulting ligands are flexible enough to accommodate a variety of metal ions in multiple oxidation states and coordination numbers.[4−9] Herein, we describe the syntheses and structures of two five-coordinate heteroleptic thiolate/N complexes containing Fe^{2+} and Co^{2+} in approximately the same distorted five-coordinate S_2N_3 environment (Scheme 1). The Zn^{2+} and Ni^{2+} analogues were previously reported by us.[4,5] The selection of metal ions examined in this study was based on their biological significance. Thiolate(S^{cys})/nitrogen(peptide amide)-ligated Fe^{2+} has been proposed to be present in the inactive form of the metalloenzyme nitrile hydratase (NHase),[10,11] an enzyme which converts nitriles to amides.[12,13] Cobalt is found to replace iron in some bacterial species containing this enzyme.[12,14] Thiolate(S^{cys})/nitrogen-ligated Ni^{2+} is found in carbon monoxide dehydrogenase (CODH),[15,16] an enzyme which reversibly forms C−C bonds in acetate synthesis, and S^{cys}-ligated Ni^{2+} is found in hydrogenase,[17,18] a metalloenzyme which activates H_2. Thus, we can compare the properties of a series of structurally analogous complexes containing metal ions in biologically relevant environments.

Another challenge in the field of bioinorganic chemistry involves the understanding of the subtle effects that protein

(1) Holm, R. H.; Kennepohl, P.; Solomon, E. I. *Chem. Rev.* **1996**, *96*, 2239−2314.
(2) Coucouvanis, D.; Swenson, D.; Baenziger, N. C.; Murphy, C.; Holah, D. G.; Sfarnas, N.; Simopoulos, A.; Kostikas, A. *J. Am. Chem. Soc.* **1981**, *103*, 3350−3362.
(3) Holm, R. H.; Ibers, J. A. In *Iron−Sulfur Proteins*; Lovenberg, W., Ed.; Academic Press: New York, 1977; Vol. III.; Chapter 7.
(4) Shoner, S. C.; Olmstead, M. M.; Kovacs, J. A. *Inorg. Chem.* **1994**, *33*, 7−8.
(5) Shoner, S; Humphreys, K.; Barnhart, D.; Kovacs J. A. *Inorg. Chem.* **1995**, *34*, 5933−5934.
(6) Shoner, S.; Barnhart, D.; Kovacs, J. A. *Inorg. Chem.* **1995**, *34*, 4517−4518.
(7) Schweitzer, D.; Ellison, J. J.; Shoner, S. C.; Lovell, S.; Kovacs, J. A., *J. Am. Chem. Soc.* **1998**, *120*, 0000 (in press).
(8) Jackson, H. L.; Kovacs, J. A., unpublished results.
(9) Ellison, J. J.; Nienstedt, A.; Shoner, S. C.; Barnhart, D.; Cowen, J. A., Kovacs, J. A. *J. Am. Chem. Soc.* **1998**, *120*, 5691−5700.
(10) Honda, J.; Teratani, Y.; Kobayashi, Y.; Nagamune, T.; Sasabe, H.; Hirata, A.; Ambe, F.; Endo, I. *FEBS Lett.* **1992**, *301*, 177−180.
(11) Noguchi, T.; Honda, J.; Nagamune, T.; Sasabe, H.; Inoue, Y.; Endo, I. *FEBS Lett.* **1995**, *358*, 9−12.
(12) Brennan, B. A.; Alms, G.; Scarrow, R. C. *J. Am. Chem. Soc.* **1996**, *118*, 9194.
(13) Scarrow, R. C.; Brennan, B. A.; Nelson, M. J. *Biochemistry* **1996**, *35*, 10078−10088.
(14) Pogorelova, T. E.; Ryabchenko, L. E.; Yanenko, A. S. *FEMS Microbiol Lett.* **1996**, *144*, 191.
(15) Ragsdale, S. W.; Kumar, M. *Chem. Rev.* **1996**, *96*, 2515−2540.
(16) Kovacs, J. A.; Shoner, S. C.; Ellison, J. J. *Science* **1995**, *270*, 587−588.
(17) Fentecilla-Camps, J. C. *J. Biol. Inorg. Chem.* **1996**, *1*, 91−98.
(18) Kovacs, J. A. Understanding the Role of Ni in Ni-Containing Enzymes. In *Advances in Inorganic Biochemistry*; Eichhorn, G. L., Marzilli, L. G., Eds.; Prentice Hall: Englewood Cliffs, NJ, 1994; Vol. 9, Chapter 5, pp 173−201.

10.1021/ic980882r CCC: $15.00
Published on Web 10/10/1998

constraints can have on geometric structure and reactivity of metalloenzyme active sites. Protein constraints have been shown to influence metal ion geometric and electronic structure[19] and have been proposed to influence reactivity by holding the metal in an approximately transition-state structure (the entatic state).[1,20,21] The metal complexes described herein incorporate a linear chain ligand which constrains the angles about the metal and thereby influences metal ion geometry. The influences that these constraints have on reactivity are explored in a separate paper.[9]

Experimental Section

General Methods. Unless noted otherwise, all reactions were carried out under dinitrogen at room temperature using Schlenk line or drybox techniques. Solvents were dried over calcium hydride (MeCN), sodium/benzophenone (Et_2O), and magnesium turnings (MeOH, EtOH); freshly distilled under dinitrogen; and degassed prior to use. 3-Methyl-3-chloro-2-butanone[22] and 2,5-dimethyl-2,5-dihydroxy-1,4-dithiane (α-mercaptoacetone dimer)[23] were synthesized by literature procedures. Anhydrous $FeCl_2$ (Aldrich), anhydrous $CoCl_2$ (Aldrich), and *N*-(3-aminopropyl)-1,3-propanediamine (Aldrich) were used as received. NMR spectra were recorded on Bruker AC-200, AF-300, and VXR-500 spectrometers. IR samples were prepared as KBr pellets, and spectra were obtained using a Perkin-Elmer 1600 FT-IR spectrometer. A Hewlett-Packard model 8450 spectrometer interfaced to an IBM PC was used to record UV/vis/near-IR spectra. Magnetic moments were determined in solution using the Evans method,[24] as corrected for superconducting solenoids.[25] Elemental analyses were performed by either Galbraith Labs or Canadian Microanalytical Service.

3-Methyl-3-mercapto-2-butanone. Sodium hydroxide (8 g, 200 mmol) was dissolved in 100 mL of MeOH. This solution was degassed and cooled to −15 °C and then saturated with H_2S. 3-Methyl-3-chloro-2-butanone[22] (24.1 g, 200 mmol) was added dropwise to this solution over 1 h, resulting in the formation of a white precipitate (NaCl). The mixture was warmed to −5 °C and stirred for 1 h and then warmed to room temperature and stirred for an additional hour. An aqueous acidic solution (H_2O/H_2SO_4, pH = 4, 100 mL) was then added, and the product was extracted with CH_2Cl_2 (4 × 25 mL). The extract was dried over $MgSO_4$ and then filtered. MeOH and CH_2Cl_2 were removed by distillation at ambient pressure. 3-Methyl-3-mercapto-2-butanone was then isolated, as a foul smelling colorless liquid, by distillation at 85 °C under reduced pressure. Yield: 18.2 g (77%). ^{1}H NMR ($CDCl_3$): δ 1.48 (6, CH_3), 2.01(1, SH), 2.30 (3, CH_3). ^{13}C NMR ($CDCl_3$): δ 23.75, 27.68, 50.29, 207.38.

[$Fe^{II}S_2N_3$(Pr,Pr)]·EtOH (1). The α-mercaptoacetone dimer, 2,5-dimethyl-2,5-dihydroxy-1,4-dithiane (0.54 g, 3 mmol),[23] was combined with sodium methoxide (0.32 g, 6 mmol) in MeOH (20 mL) and then added dropwise to a solution containing anhydrous $FeCl_2$ (0.38 g, 3 mmol) in MeOH (10 mL) at 12 °C. This resulted in a red solution. After 30 min of stirring, *N*-(3-aminopropyl)-1,3-propanediamine (0.39 g, 3 mmol) was added. The resulting chartreuse green solution was stirred for an additional 2 h, at which time all volatiles were removed under vacuum. The green solid was extracted with EtOH (20 mL) and then filtered over Celite to remove NaCl along with black insoluble impurities. The filtrate volume was reduced to 5 mL, and the solution was then layered with Et_2O (25 mL), resulting in the formation of [$Fe^{II}S_2N_3$(Pr,Pr)]·EtOH ((1,2-dimethyl-3,7,1-triazatridecane-1,13-dithiolato)iron(II)−ethanol) as a light chartreuse green microcrystalline solid. Yield: 0.49 g, (44%). Absorption spectra: (MeOH) λ_{max} (ϵ_M) = 376 (930) nm; (H_2O) λ_{max} (ϵ_M) = 359 (820) nm; (MeCN) λ_{max} (ϵ_M) = 396 (860) nm. Ambient temperature (297 K) μ_{eff} = 5.15 μ_B in MeOH solution. IR ν (cm^{-1}): 1637 (imine). Anal. Calcd for $FeC_{12}H_{23}N_3S_2$: C, 43.77; H, 7.04; N, 12.76. Found: C, 43.36; H, 6.95; N, 12.63.[26] ^{1}H NMR spectra (CD_3OD): δ 292, 282, 280, 241, 218, 166, 154, 98, 92, 52, 40, 33, 30, 20, −4, −11, −26, −60. D_2O: δ 318, 267, 264, 263,224, 157, 137, 98, 92, 54, 48, 36, 30, 18, −4, −8, −28, −59. CD_3CN: δ 249, 222, 216, 211, 209, 203, 189, 111, 95, 81, 36 (CH_3), 35 (CH_3), 23, −4, −14−32, −68.

[$Co^{II}S_2^{Me2}N_3$(Pr,Pr)]·CH_3CN (2). A cold (ca. −20 °C) mixture of 3-methyl-3-mercapto-2-butanone (1.12 g, 9.5 mmol) and triethylamine (0.97 g, 9.6 mmol) in MeOH (ca. 10 mL) was added dropwise to a stirred solution of anhydrous cobalt(II) chloride (0.62 g, 4.8 mmol) in

Table 1. Crystal Data for [Fe^{II}(S_2N_3(Pr,Pr))]·EtOH (**1**) and [Co^{II}($S_2^{Me2}N_3$(Pr,Pr))]·MeCN (**2**)

	1	**2**
formula	$FeS_2N_3OC_{14}H_{29}$	$CoS_2N_4C_{18}H_{34}$
fw	375.37	429.5
unit cell[a]	monoclinic	monoclinic
a, Å	7.853(2)	9.389(2)
b, Å	8.667(2)	19.706(3)
c, Å	26.079(5)	12.165(2)
α, deg	90.0	90.0
β, deg	90.37(3)	103.67(2)
γ, deg	90.0	90.0
V, Å^3	1775.0(7)	2186(1)
Z	4	4
σ_{calc}, g/cm^3	1.405	1.305
space group	$P2_1/c$	$P2_1/c$
μ, cm^{-1}	10.87	9.84
transmission factors	0.9993−0.4975[b]	0.9773−0.8907[b]
R[c]	0.045	0.071
R_w	0.058	0.098
GOF	1.44	1.14

[a] In all cases: Mo Kα̅ (λ = 0.710 73 Å) radiation; graphite monochromator; −90 °C. [b] A semiempirical absorption correction was applied. [c] $R = \sum||F_o| - |F_c||/\sum|F_o|$; $R_w = [\sum w(|F_o| - |F_c|)^2/\sum wF_o^2]^{1/2}$, where $w^{-1} = [\sigma^2_{count} + (0.05F^2)^2]/4F^2$.

Table 2. Selected Bond Distances (Å) and Angles (deg) for [Fe^{II}(S_2N_3(Pr,Pr))] (**1**)

Fe(1)−S(1)	2.363(1)	Fe(1)−S(2)	2.342(1)
Fe(1)−N(1)	2.168(3)	Fe(1)−N(2)	2.181(3)
Fe(1)−N(3)	2.183(4)	S(1)−C(1)	1.821(5)
S(2)−C(11)	1.812(5)	N(1)−C(2)	1.280(5)
N(1)−C(4)	1.469(5)	N(2)−C(6)	1.484(5)
N(2)−C(7)	1.486(6)	N(3)−C(9)	1.465(7)
N(3)−C(10)	1.273(6)	C(1)−C(2)	1.497(6)
C(2)−C(3)	1.503(6)	C(4)−C(5)	1.528(6)
C(5)−C(6)	1.524(6)	C(7)−C(8A)	1.539(9)
C(7)−C(8B)	1.478(12)	C(8B)−C(9)	1.400(13)
C(8A)−C(9)	1.392(12)	C(10)−C(12)	1.519(6)
C(10)−C(11)	1.497(6)		
S(1)−Fe(1)−S(2)	124.3(1)	S(1)−Fe(1)−N(1)	82.9(1)
S(2)−Fe(1)−N(1)	104.7(1)	S(1)−Fe(1)−N(2)	121.6(1)
S(2)−Fe(1)−N(2)	114.0(1)	N(1)−Fe(1)−N(2)	87.6(1)
S(1)−Fe(1)−N(3)	101.7(1)	S(2)−Fe(1)−N(3)	82.3(1)
N(1)−Fe(1)−N(3)	167.7(1)	N(2)−Fe(1)−N(3)	80.3(1)
Fe(1)−S(1)−C(1)	98.1(1)	Fe(1)−S(2)−C(11)	99.9(1)
Fe(1)−N(1)−C(2)	120.0(3)	Fe(1)−N(1)−C(4)	120.9(3)
C(2)−N(1)−C(4)	119.0(3)	Fe(1)−N(2)−C(6)	115.0(2)
Fe(1) −N(2)−C(7)	116.2(3)	C(6)−N(2)−C(7)	111.2(3)
Fe(1)−N(3)−C(9)	116.8(3)	Fe(1)−N(3)−C(10)	121.3(3)
C(9)−N(3)−C(10)	121.7(4)	S(1)−C(1)−C(2)	116.2(3)
N(1)−C(2)−C(1)	120.4(3)	N(1)−C(2)−C(3)	124.9(4)
C(1)−C(2)−C(3)	114.7(3)	N(1)−C(4)−C(5)	110.9(3)
C(4)−C(5)−C(6)	112.3(4)	N(2)−C(6)−C(5)	109.7(3)
N(2)−C(7)−C(8A)	110.3(4)	N(2)−C(7)−C(8B)	116.3(5)
C(7)−C(8A)−C(9)	118.9(6)	C(7)−C(8B)−C(9)	122.6(8)
N(3)−C(9)−C(8B)	118.0(6)	N(3)−C(9)−C(8A)	113.3(5)
N(3)−C(10)−C(11)	119.7(4)	N(3)−C(10)−C(12)	123.9(4)
C(11)−C(10)−C(12)	116.3(4)	S(2)−C(11)−C(10)	116.3(3)

(19) Colman, P. M.; Freeman, H. C.; Guss, J. M.; Murata, M.; Norris, V. A.; Ramshaw, J. A. M.; Venkatappa, M. P. *Nature* **1978**, *272*, 319.
(20) Vallee, B. L.; WIlliams, R. J. P. *Proc. Natl. Acad. Sci. U.S.A.* **1968**, *59*, 498.
(21) Malmstrom, B. G. *Eur. J. Biochem.* **1994**, *223*, 711.
(22) Wyman, D. P.; Kaufman, P. R. *J. Org. Chem.* **1964**, *29*, 1956.
(23) Hromatka, O.; Engel, E. *Monatsh. Chem.* **1948**, *78*, 29.
(24) Evans, D. A. *J. Chem. Soc.* **1959**, 2005.
(25) Live, D. H.; Chan, S. I. *Anal. Chem.* **1970**, *42*, 791.

Table 3. Selected Bond Distances (Å) and Angles (deg) for $[Co^{II}S_2{}^{Me2}N_3(Pr,Pr)]$ (**2**)

Co−S(1)	2.293(1)	C(1)−C(2)	1.517(6)
Co−S(2)	2.278(2)	C(1)−C(11)	1.544(7)
Co−N(1)	2.127(4)	C(1)−C(12)	1.535(7)
Co−N(2)	2.141(4)	C(2)−C(13)	1.517(7)
Co−N(3)	2.109(4)	C(3)−C(4)	1.515(8)
S(1)−C(1)	1.829(4)	C(4)−C(5)	1.510(8)
S(2)−C(10)	1.831(5)	C(6)−C(7)	1.489(6)
N(1)−C(2)	1.271(6)	C(7)−C(8)	1.526(6)
N(1)−C(3)	1.475(6)	C(9)−C(10)	1.531(7)
N(2)−C(5)	1.459(6)	C(9)−C(16)	1.513(8)
N(2)−C(6)	1.483(7)	C(10)−C(14)	1.535(7)
N(3)−C(8)	1.459(6)	C(10)−C(15)	1.535(6)
N(3)−C(9)	1.258(6)		
S(1)−Co−S(2)	126.6(1)	S(1)−C(1)−C(2)	111.9(3)
S(1)−Co−N(1)	83.0(1)	S(1)−C(1)−C(11)	108.3(3)
S(2)−Co−N(1)	105.6(1)	C(2)−C(1)−C(11)	111.4(4)
S(1)−Co−N(2)	120.2(1)	S(1)−C(1)−C(12)	109.2(3)
S(2)−Co−N(2)	112.6(1)	C(2)−C(1)−C(12)	106.5(4)
N(1)−Co−N(2)	89.7(1)	C(11)−C(1)−C(12)	109.5(4)
S(1)−Co−N(3)	96.3(1)	N(1)−C(2)−C(1)	120.6(4)
S(2)−Co−N(3)	82.6(1)	N(1)−C(2)−C(13)	122.9(4)
N(1)−Co−N(3)	170.3(1)	C(1)−C(2)−C(13)	116.5(4)
N(2)−Co−N(3)	82.2(1)	N(1)−C(3)−C(4)	110.9(4)
Co−S(1)−C(1)	100.1(1)	C(3)−C(4)−C(5)	113.3(5)
Co−S(2)−C(10)	102.3(2)	N(2)−C(5)−C(4)	111.5(4)
Co−N(1)−C(2)	120.7(3)	N(2)−C(6)−C(7)	112.4(4)
Co−N(1)−C(3)	120.0(3)	C(6)−C(7)−C(8)	115.8(4)
C(2)−N(1)−C(3)	119.3(4)	N(3)−C(8)−C(7)	109.5(3)
Co−N(2)−C(5)	114.4(3)	N(3)−C(9)−C(10)	119.9(4)
Co−N(2)−C(6)	111.1(3)	N(3)−C(9)−C(16)	123.6(5)
C(5)−N(2)−C(6)	112.2(4)	C(10)−C(9)−C(16)	116.4(4)
Co−N(3)−C(8)	113.8(3)	S(2)−C(10)−C(9)	111.6(3)
Co−N(3)−C(9)	123.2(3)	S(2)−C(10)−C(14)	108.8(3)
C(8)−N(3)−C(9)	122.3(4)	C(9)−C(10)−C(14)	108.6(4)
		S(2)−C(10)−C(15)	109.3(4)
		C(9)−C(10)−C(15)	109.1(4)
		C(14)−C(10)−C(15)	109.5(4)

MeOH (ca. 35 mL) to afford a deeply colored magenta solution and a burgundy microcrystalline precipitate. The dropwise addition to this reaction mixture of *N*-(3-aminopropyl)-1,3-propanediamine (0.62 g, 4.8 mmol) dissolved in MeOH (10 mL) caused the solid to redissolve and afforded a deep purple solution. The resulting reaction mixture was then stirred at ambient temperature for 12 h. The volatiles were removed under vacuum, and the resulting dark purple residue was redissolved in MeCN (ca. 10 mL) and filtered to remove a black impurity. This MeCN solution was then layered with Et_2O (ca. 80 mL) and cooled to −20 °C to afford 0.336 g (16%) of $[Co^{II}S_2N_3{}^{Me2}(Pr,Pr)]\cdot CH_3CN$ (2,3,13,14-tetramethyl-4,8,12-triaza-3,12-pentadecadien-2,14-dithiolato)cobalt(II)−acetonitrile) as a purple microcrystalline solid. Absorption spectra: (MeOH) λ_{max} (ϵ_M) = 290 (4900), 350 (3000), 488 (49), 564 (56) nm; (H_2O) λ_{max} (ϵ_M) = 288 (4900), 338 (3000), 488 (48), 576 (56) nm; (MeCN) λ_{max} (ϵ_M) = 298 (4800), 362 (3800), 496 (62), 536 (66). μ_{eff} = 4.32 μ_B in MeCN solution (298 K). IR ν (cm^{-1}): 1651, 1632 (imine). Anal. Calcd for $CoC_{16}H_{31}N_3S_2$: C, 49.46; H, 8.04; N, 10.81. Found: C, 49.19; H, 7.90; N, 10.62.[26] ^1H NMR (CD_3CN): δ 275, 212, 151, 111, 68, 46 (CH_3), 43 (CH_3), 39, 23, 16, 13, −13, 15, −18 ($CH_3 \times 2$), −22, −33 ($CH_3 \times 2$). ^1H NMR (CD_3OD): δ 311, 234, 158, 118, 45(CH_3), 40, 37(CH_3), 32, 30, 17, 13, 11, −12 ($CH_3 \times 2$), −17 ($CH_3 \times 2$), −19, −21, −35. D_2O: δ 333, 249, 156, 125, 44, 43 (CH_3), 40, 37 (CH_3), 31, 14, 11, −10, −16 ($CH_3 \times 2$), −17, −20, −32 ($CH_3 \times 2$).

X-ray Crystallographic Structure Determinations. Crystals of **1** and **2** were immersed in oil inside a drybox, and a suitable crystal was then mounted on a glass fiber with silicon grease and immediately placed in a low-temperature N_2 stream. X-ray data were collected at −90 °C using an Enraf-Nonius CAD4 diffractometer (Mo Kα, λ = 0.710 69 Å) equipped with a low-temperature device. Calculations were carried out on either a Gateway 2000 486DX2150 computer with XCAD4 SHELX PLUS (PC version) software or a MicroVAX computer with MOLen software. Scattering factors were from taken from a standard source.[27] A ψ scan absorption correction of a high χ reflection was performed for both compounds. X-ray data collection parameters are summarized in Table 1.

Yellow-green X-ray quality plates of **1**·EtOH were grown from a cooled (−20 °C) concentrated EtOH solution of **1**. Purple X-ray quality rhombs of **2**·MeCN were grown from a concentrated MeCN solution of **2** layered with Et_2O. Twenty-five reflections in the range 2θ = 30−40° were found and centered to determine the cell constants and orientation matrixes for both **1** and **2**. Standard reflections examined after every 200 reflections for **1** showed no signs of decay. For **2**, the crystal moved during data collection, requiring that it be recentered and a scaling factor be applied. The poor *R* value (0.071(0.098)) obtained for **2** may be due to the failure of this correction to account for systematic statistical errors. The systematic absences *h*0*l* ($l = 2n + 1$) and 0*k*0 ($k = 2n + 1$) uniquely define the space group of both **1** and **2** as $P2_1/c$. The semiempirical absorption correction for **1** was unusually large due to the plate shape of the crystal. Therefore, a spherical correction was also applied for **1**. Data reduction was carried out using MOLen, and further calculations were carried out using SHELX PLUS (PC version). The iron atom of **1** was located using a Patterson function, and the remaining atoms were located using difference maps from subsequent least-squares refinement. The cobalt atom of **2** was located by direct methods, and the remaining atoms were located using difference maps from subsequent least-squares refinement. An EtOH and a MeCN solvent molecule were located during the later stages of refinement of **1** and **2**, respectively. Allhydrogen atoms, except for the ethanolic proton of **1**, were included

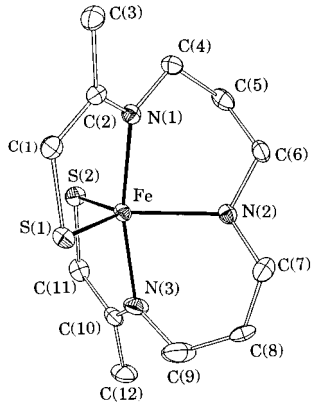

Figure 1. ORTEP plot of $[Fe^{II}S_2N_3(Pr,Pr)]$ (**1**) showing 40% probability ellipsoids and atom labeling scheme. H atoms have been omitted for clarity.

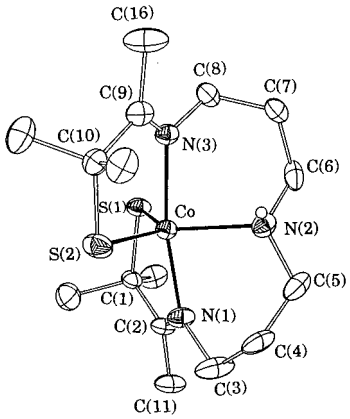

Figure 2. ORTEP plot of $[Co^{II}S_2{}^{Me2}N_3(Pr,Pr)]$ (**2**) showing 50% probability ellipsoids and atom labeling scheme. All H atoms except the N(2)−H proton have been omitted for clarity.

(26) Analyses were most consistent with a desolvated form.

(27) Cromer, D. T.; Waber, J. T. In *International Tables for X-ray Crystallography*; Kynoch: Birmingham, England, 1974; Vol. IV.

Table 4. Comparison of Selected Metrical Parameters for Five-Coordinate $[M^{II}S_2{}^{R2}N_3(Pr,Pr)]$; M = Fe (**1**), Co (**2**), Ni (**3**), and Zn (**4**)

	1·EtOH	**2**·MeCN	**3**	**4**·MeOH
M−S(1)	2.363(1) Å[a]	2.293(1) Å	2.306(2) Å	2.337(1) Å
M−S(2)	2.342(1) Å	2.278(2) Å	2.359(2) Å[b]	2.329(1) Å[a]
M−N(1)	2.168(3) Å	2.127(4) Å	2.065(4) Å	2.167(3) Å
M−N(3)	2.183(4) Å	2.109(4) Å	2.048(4) Å	2.179(3) Å
M−N(2)	2.181(3) Å	2.141(4) Å	2.068(3) Å	2.142(4) Å
N(1)−M−N(3)	167.7(1)°	170.3(1)°	177.3(2)°	170.0(1)°
S(1)−M−S(2)	124.3(1)°	126.6(1)°	135.3(1)°	124.1(1)°
S(2)−M−N(2)	114.0(1)°	112.6(1)°	101.0(1)°	117.2(1)°
S(1)−M−N(2)	121.6(1)°	120.2(1)°	123.4(1)°	118.4(1)°
N(1)−M−S(1)	82.9(1)°	83.0(1)°	84.7(1)°	86.3(1)°
N(1)−M−S(2)	104.7(1)°	105.6(1)°	99.1(1)°	90.5(1)°
N(1)−M−N(2)	87.6(1)°	89.7(1)°	92.7(1)°	94.7(1)°
N(3)−M−S(1)	101.7(1)°	96.3(1)°	93.4(1)°	98.2(1)°
N(3)−M−S(2)	82.3(1)°	82.6(1)°	83.6(1)°	83.9(1)°
N(3)−M−N(2)	80.3(1)°	82.2(1)°	86.7(1)°	81.9(1)°
ligand wrapping angle[c]	484.3°	486.6°	495.3°	484.1°
helicity angle (ϕ)[c]	33.2°	43.1°	69.3°	33.2°

[a] This sulfur is H-bonded to an alcohol with an S···H(OR) separation of 2.41(5) Å in **1** and 2.34(6) Å in **4**. [b] This sulfur is H-bonded to an adjacent molecule in the unit cell with an S···H−N separation of 3.02(5) Å. [c] See text for definition of these angles.

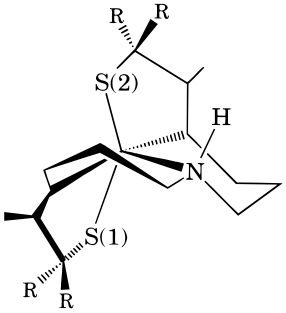

Figure 3. MacMolecule stick figure of $[M^{II}S_2{}^{Rz}N_3(Pr,Pr)]$ depicting chelate ring conformations. SHELX crystallographic positional parameters (for M = Fe), in an orthogonal coordinate system, were used to generate this figure.

in calculated positions and refined using a riding model. The ethanolic proton of **1** was located in a difference map, and its position was refined for four least-squares cycles and then fixed. For **1**, C(8) was found to be 50:50 disordered between two positions. All non-hydrogen atoms were refined anisotropically for both **1** and **2**. The final full-matrix least-squares refinement of **1**, with 200 parameters and 2519 reflections all having $F > 4.0\sigma(F)$, converged with an *R* factor of 4.5%. The final full-matrix least-squares refinement of **2**, with 226 parameters and 3107 reflections all having $F > 4.0\sigma(F)$, converged with an *R* factor of 7.1%. Selected bond distances and angles for compounds **1** and **2** are summarized in Tables 2 and 3, respectively.

Results and Discussion.

Synthesis. Thiolate-ligated $[Fe^{II}S_2N_3(Pr,Pr)]$ (**1**) and $[Co^{II}S_2{}^{Me2}N_3(Pr,Pr)]$ (**2**) were prepared using a "one-pot" synthesis involving a metal-templated Schiff base condensation between *N*-(3-aminopropyl)-1,3-propanediamine and 2 equiv of a deprotonated α-mercapto ketone in MeOH solution (Scheme 1). A similar procedure was used to synthesize the nickel and zinc analogues, $[Ni^{II}S_2N_3(Pr,Pr)]$ (**3**)[4] and $[Zn^{II}S_2N_3(Pr,Pr)]$·MeOH (**4**).[5] This generalized procedure can be used to synthesize mixed thiolate/amine/imine-ligated transition-metal complexes with a wide variety of structures.[4−9] Compounds **1** and **2** are extremely sensitive to even trace amounts of oxygen. To avoid extensive decomposition, reactions were run at low temperatures, and the products were isolated within hours of their preparation. Steric protection in the form of *gem*-dimethyls adjacent to the thiolate sulfurs was used to increase the stability of the cobalt complex **2**, the least stable of the four complexes discussed in this paper. *gem*-Dimethyl protection has also recently been used by our group to stabilize thiolate-ligated Fe^{3+} in a coordinatively unsaturated environment.[9]

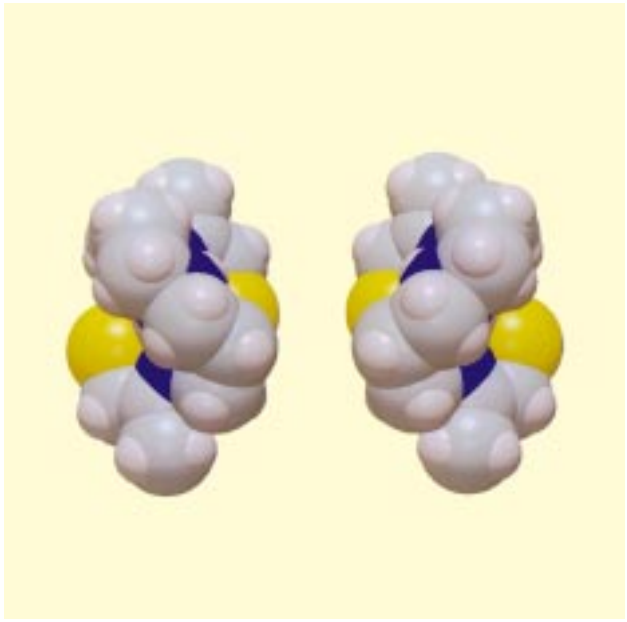

Figure 4. Space-filling drawings of the right-handed and left-handed isomers of $[M^{II}S_2N_3(Pr,Pr)]$ depicting their helical structure. Molscript (Kraulis, P. J. *J. Applied Crystallogr.* **1991**, *24*, 946) and Raster3D (Merritt, E. A.; Murphy, M. *Acta. Crystallogr.* **1994**, *D50*, 869.) were used to generate this figure, using crystallographic coordinates of **1**.

Figure 5. Helicity angle ϕ as depicted by a MacMolecule drawing of $[M^{II}S_2N_3(Pr,Pr)]$. SHELX crystallographic positional parameters (for M = Fe) were used to generate this figure.

Scheme 1

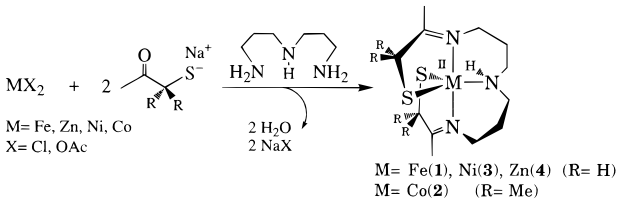

X-ray Structures. Single crystals of **1**·EtOH and **2**·MeCN were isolated from Et_2O-layered EtOH and MeCN solutions, respectively. Both **1** and **2** are neutral in charge, as are $[Ni^{II}S_2N_3(Pr,Pr)]$ (**3**)[4] and $[Zn^{II}S_2N_3(Pr,Pr)]$·MeOH (**4**).[5] ORTEP diagrams of **1** and **2** are shown in Figures 1 and 2, respectively, and distances and angles are contained in Tables

2 and 3. Metrical parameters for the iron (**1**), cobalt (**2**), nickel (**3**), and zinc (**4**) complexes derived from the $[(Pr,Pr)N_3(S)_2]^{2-}$ or $[(Pr,Pr)N_3(S^{Me2})_2]^{2-}$ ligands are compared in Table 4. Compounds **1**−**4** have been given a consistent numbering system.

Metal Ion Geometry. The metal ions in iron- or cobalt-containing **1** (Figure 1) and **2** (Figure 2) are each located in a coordinatively unsaturated five-coordinate S_2N_3 environment similar to that of nickel- and zinc-containing[4,5] **3** and **4** (Scheme 1). The geometry of these structures varies from severely distorted (**3**) to nearly ideal (**4**) trigonal bipyramidal. The equatorial planes each contain two *cis*-thiolate sulfurs (S(1) and S(2)) and an amine nitrogen (N(2)). The axial sites are occupied by imine nitrogens (N(1) and N(3)). Deviations from linearity of the apical N(1)−M−N(3) angle decrease in the order **1** (12.4(1)°) > **4** (10.0(1)°) > **2** (9.7(1)°) ≫ **3** (2.7(1)°) (Table 4). Deviations from ideal geometry in the equatorial $MS_2N(2)$ plane increase in the order **4** < **1** < **2** < **3**; angles range from 117.0(1)° to 124.1(1)° in **4**, 114.0(1)° to 124.3(1)° in **1**, 112.6(1)° to 126.6(1)° in **2**, and 101.0(0)° to 135.3(1)° in **3** (Table 4). Possible causes for these distortions include (1) ligand constraints and/or (2) intramolecular S···H−N(2) H-bonding forces.

Chelate Rings. Two five-membered (−M−S−CH_2−CH═N−) and two six-membered (−M−N−Pr−N(H)−) rings make up the pentadentate chelate of these structures. The two six-membered rings share a common nitrogen (N(2)−H). The N(1)−Pr−N(2)H chelate ring adopts a twisted boat conformation (Figure 3) in **1**−**4**, while the N(3)−Pr−N(2)H chelate ring adopts a chair conformation[28] in **2**−**4** (this ring is disordered in structure **1**). This is the usual conformational arrangement (twisted boat/chair) observed with structures containing two fused six-membered X−Pr−X chelate rings (X = N, O, S)[29−32] and is the only arrangement which will allow the three heteroatoms involved to occupy meridional positions about the metal ion. This arrangement also places the N(2)−H proton in an axial "cyclohexyl" position so that it points away from S(1) and toward S(2). This is how S(2) was defined in structures **1**−**4**, as the sulfur toward which the N(2)−H proton points. S···H−N(2) separations fall outside the sum of their van der Waals radii (3.05 Å)[33] in all four structures (3.40(5) Å in **2**, 3.55(5) Å in **1**, 3.58(5) Å in **4**, and 3.16(5) Å in **3**), ruling out intramolecular H-bonding as a possible cause for the observed distortions in these structures.

Coiling of the Helical Ligand. The $[S_2{}^{R2}N_3(Pr,Pr)]^{2-}$ ligands wrap around the +2 metal ions in **1**−**4** in a helical fashion (as shown in Figure 4) to afford chiral helical molecules with approximately C_2 symmetry. Both enantiomers are present in all four structures in a 1:1 ratio and are related by a crystallographic inversion center. One can describe the extent of helical coiling in these structures **1**−**4** in terms of a "helicity angle"[34] which is defined as the dihedral angle (ϕ shown in Figure 5) between the inclined FeN(2)C(6)C(7) or CoN(2)C(5)C(6) plane (carbons C(5), C(6), and C(7) are the labeled in the ORTEP diagrams of Figures 1 and 2) and the vertical MN(1)N(3) plane. This angle increases monotonically in the order **4** (33.2°) = **1** (33.2°) < **2** (43.1°) ≪ **3** (69.3°) (Table 4), with the most dramatic increase occurring between the Co and Ni complexes. This trend correlates with the ionic radii, (Fe^{2+} (0.84 Å) ≥ Zn^{2+} (0.82 Å) ≥ Co^{2+} (0.81 Å) ≫ Ni^{2+} (0.77 Å)).[35] Angular distortions in the equatorial plane of **1**−**3** also correlate with ϕ: as ϕ increases the structure becomes more severely distorted. Alternatively, one can describe the extent of helical coiling in these structures in terms of a ligand "wrapping angle" which we define as 360° plus or minus the dihedral angle spanned by the M−S(1) and M−S(2) bond vectors as viewed along a normal to the ~C_2 axis (see molecular orientation shown in Scheme 1). In all four complexes, the ligand wraps around the metal ion slightly more than once, i.e., the wrapping angles are all greater than 360° (Table 4). This angle also increases monotonically from **1** to **3**, with the most dramatic increase occurring at Ni. In structures **4** and **1**, this angle is approximately the same. This trend also correlates with ionic radius and angular distortions in the equatorial plane.

Ligand Constraints. Energy minimized "Chem 3D"[36] models demonstrate that one of the equatorial S−M−N angles in structures **1**−**4**, S(2)−M−N(2), is sensitive to changes in the mean apical M−N(1,3) distance and closes dramatically in response to decreases in this distance. If one cuts the ligand into two parts, using this program, then the S(2)−M−N(2) angle springs back to its idealized ~120° value. These simulations indicate that ligand constraints could be responsible for the observed angular distortions in the equatorial $MS_2N(2)$ plane. This is supported by the X-ray structural data. As shown in Table 4, the S(2)−M−N(2) angle decreases monotonically from **1** to **3** as the M−N(1,3) distances decrease, with the most dramatic decrease occurring between the Co and Ni complexes. The distances in the Zn structure **4** are most similar to **1** and result in the least distorted angles. Constraints are placed on the allowable combinations of M−N(S) distances and N(S)−M−N(S) angles, because the multidentate ligand $[S_2{}^{R2}N_3(Pr,Pr)]^{2-}$ has a fixed length. As the metal−ligand distances change in response to changes in the metal ion (Table 4) or its oxidation state,[9] the angles about the metal ion distort so as to conform to the ligand's fixed length. Some of these angle changes are absorbed by the Pr carbon chains (Tables 2 and 3); however, because bonding is more flexible to the metal, it withstands most of the distortion. The angles which are most affected by these constraints are the apical N(1)−M−N(3) and equatorial S−M−N(2) angles (Table 4). A more dramatic example of this is seen upon oxidation of a *gem*-dimethyl protected derivative of **1**.[9] Comparison of the reduced and oxidized structures, $[Fe^{II}S_2N_3(Pr,Pr)]$ (**1**) and $[Fe^{III}S_2{}^{Me2}N_3(Pr,Pr)]^+$ (**5**), shows that the metal−ligand bond lengths decrease, causing the apical N(1)−M−N(3) angle to increase (from 167.7(1)° in **1** to 178.1(2)° in **5**) and the S(2)−Fe−N(2) angle to decrease (from 114.0(1)° in **1** to 106.5(1)° in **5**) in response to oxidation.[9] The S(1)−Fe−N(2) angle opens (from 121.6(1)° in **1** to 132.3(1)° in **5**) in response to the other S−Fe−N angle closing. Azide[9] and nitric oxide[7] were found to bind to the open angle of **5**.

Metal−Ligand Distances. The mean M−N distance in the $[M^{II}(S^{R2}N_3(Pr,Pr)]$ (M = Fe (**1**), Co (**2**), Ni (**3**), Zn (**4**); R = H, Me) structures decreases monotonically (Table 4) from **1** to **3**

(28) If one is to apply the nomenclature pertaining to all-carbon ring systems.
(29) DaCruz, M. F.; Zimmer, M. *Inorg. Chem.* **1998**, *37*, 366−368.
(30) Freyberg, D. P.; Mockler, G. M.; Sinn, E. *J. Chem. Soc. Dalton Trans.* **1976**, 447.
(31) Cini, R.; Orioli, P. *Inorg. Chim. Acta* **1982**, *63*, 243.
(32) Zanello, P.; Cini, R.; Cinquantinin, A.; Orioli, P. *J. Chem. Soc., Dalton Trans.* **1983**, 2159.
(33) Pauling, L. *The Nature of the Chemical Bond*, 3rd ed.; Cornell University Press: Ithaca, NY, 1960.
(34) Purcell, K. F.; Kotz, J. C. In *Inorganic Chemistry*; Saunders: Philadelphia, 1977; p 641.
(35) Shannon, R. D. *Acta Crystallogr.* **1976**, *A32*, 751. The quoted radii all pertain to M^{2+} ions in a five-coordinate environment. Since a five-coordinate radius was not available for Fe^{2+}, the 0.70 Å value quoted was computed by taking the average between a six-coordinate radius and a four-coordinate radius.
(36) Chem 3D Plus; Cambridge Scientific Computing Inc.: Cambridge, MA, version 3.1.

and follows the trend (**1** > **2** ≫ **3**) predicted based on ionic radii (with distances in **1** approximately equivalent to those in **4**). Although the number of structures available for comparison is limited (five-coordinate structures are rare), these distances fall in the usual range (2.071(4)−2.27(3) Å for Fe^{2+}; 2.037(6)−2.212(7) Å for Zn^{2+}; 2.036(4)−2.146(8) Å for Co^{2+}; 2.01(1)−2.131(6) Å for Ni^{2+}).[30,37−48] Trends in the mean M−S distance in structures **1**−**4** (**1** ≥ **4** = **3** > **2**) do not follow the order predicted on the basis of covalent (**2** ≥ **1** ≫ **3** > **4**)[49] or ionic (**1** ≥ **4** > **2** ≫ **3**) radii,[35] implying that the nature of the M−SR bonds changes through the series. On the basis of a comparison of these distances (2.35(1) Å in **1**, 2.33(1) Å in **4**, 2.33(3) Å in **3**, and 2.28(1) Å in **2**) with those predicted from covalent (2.27 Å in **1**, 2.22 Å in **4**, 2.23 Å in **3**, and 2.28 Å in **2**) or ionic (2.54 Å in **1**, 2.52 Å in **4**, 2.51 Å in **2**, and 2.47 Å in **3**) radii, it would appear that all of these have significant covalent character (∼60% in **3** and **4**, ∼70% in **1**, and ∼100% in **2**).

Iron−sulfur distances (Table 2) in **1** fall in the usual range (2.31−2.37 Å) for $S = 2$, high-spin iron thiolates.[2,43,50] There is a closer match between **1** and four-coordinate $S = 2$ complexes than between **1** and five-coordinate $S = 1$ complexes.[51] The mean cobalt−sulfur distance in **2** (Table 3) closely matches those of $[Co^{II}(S\text{-}2,4,6\text{-}(^{i}Pr)_3\text{-}C_6H_2)_2(bpy)(MeCN)]$ (2.28(2) Å)[39] and $[Co^{II}(S\text{-}2,3,5,6\text{-}Me_4\text{-}C_6H)_3(MeCN)]^-$ (2.28(1) Å),[40] indicating that the helical ligand does not place any unusual constraints on these distances. Nickel−sulfur distances in **3** fall in the usual range (2.26−2.36 Å) for five-coordinate nickel thiolate complexes,[52,53] with Ni−S(2) falling at the long end of this range (Table 4) due to its involvement in intermolecular H-bonding.[4] The mean Zn−S distance[5] in **4** is similar to those in four-coordinate $[Zn(SPh)_4]^{2-}$ (2.35(1) Å)[54] and five-coordinate $Zn(pm\text{-}2\text{-}S)_2(py)$ (2.36(1) Å)[55] and slightly longer than those in four-coordinate $[Zn(S\text{-}2,4,6\text{-}{}^{i}Pr_3\text{-}C_6H_2)_2(bpy)]$ (2.255(4) Å)[56] and $[Zn(S\text{-}2,3,5,6\text{-}Me_4C_6H)_2(1\text{-}Me\text{-}Im)_2]$ (2.300(2) Å)[56] and five-coordinate [Zn(daco-(S)(SAc))] (2.295(3) Å).[37] The factors which govern the M−S distances in these structures are, however, complicated by the irregular presence of intermolecular (in **1**, **3**, and **4**) H-bonds to the thiolate sulfurs (Table 4).

Conclusions

A comparison of the metrical parameters of a series of helical, multidentate (N, S)-chelated transition-metal complexes $[M^{II}S_2{}^{R2}N_3(Pr,Pr)]$ (M = Fe, Co, Ni, Zn; R = H, Me) has revealed that there is a correlation among ionic radii, M−N distances, ligand helicity (ϕ), and angular distortions. Angular distortions and ligand helicity both increase in response to decreases in M−N distances, with the most dramatic change occurring at Ni. These reflect constraints placed on the allowable combinations of M−N distances and N(S)−M−N(S) angles by the fixed-length single-chain ligand. Similar constraints may alter the geometries of metalloenzyme active sites. There is no correlation between the above parameters and terminal M−S distances, suggesting that, as one would expect, the interior portion (i.e., the nitrogens) of the multidentate ligand influences the observed angular distortions the most.

Acknowledgment. We thank Henry L. Jackson, Dirk Schweitzer, and Jennifer Nehring for experimental assistance and Ellie Adman (U.W., Department of Biological Structure) for generating Figure 4. Financial support from the National Institutes of Health (GM 45881) is gratefully acknowledged.

Supporting Information Available: X-ray crystallographic files in CIF format for the structures of $[Fe^{II}S_2N_3(Pr,Pr)]\cdot EtOH$ (**1**) and $[Co^{II}S_2{}^{Me2}N_3(Pr,Pr)]$ (**2**) are available on the Internet only. Access information is given on any current masthead page.

IC980882R

(37) Goodman, D. C.; Tuntulani, T.; Farmer, P. J.; Darensbourg, M. Y.; Reibenspies, J. H. *Angew. Chem., Int. Ed. Engl.* **1993**, *32*, 116−119.
(38) Corwin, D. T., Jr.; Gruff, E. S.; Koch, S. A. *J. Chem. Soc., Chem. Commun.* **1987**, *13*, 966−967.
(39) Corwin, D. T., Jr.; Fiker, R.; Koch, S. A. *Inorg. Chem.* **1987**, *26*, 3079.
(40) Koch, S. A; Fiker, R.; Millar, M.; O'Sullivan, T. *Inorg. Chem.* **1984**, *23*, 121.
(41) Chadha, R. K.; Kumar, R.; Lopez-Grado, J. R.; Tuck, D. G. *Can. J. Chem.* **1988**, *66*, 2151.
(42) Mastopaolo, D.; Thich, J. A.; Potenza, J. A.; Schugar, H. J. *J. Am. Chem. Soc.* **1977**, *99*, 424.
(43) Govindaswamy, N.; Quarless, D. A., Jr.; Koch, S. A. *J. Am. Chem. Soc.* **1995**, *117*, 8468−8469.
(44) Goedken, V. L.; Christoph, C. G. *Inorg. Chem.* **1973**, *12*, 2316.
(45) Cha, M.; Gatlin, C. L.; Critchlow, S. C.; Kovacs, J. A. *Inorg. Chem.* **1993**, *32*, 5868−5877.
(46) Sellmann, D.; Kunstmann, H.; Moll, M.; Knoch, F. *Inorg. Chim. Acta* **1988**, *154*, 157−167.
(47) Karlin, K. D.; Rabinowitz, H. N.; Lewis, D. L.; Lippard, S. J. *Inorg. Chem.* **1977**, *16*, 3262−3267.
(48) Pohl, K.; Wieghardt, K.; Nuber, B.; Weiss, J. *J. Chem. Soc., Dalton Trans.* **1987**, 187−192.
(49) Huheey, J. E.; Keiter, E. A.; Keiter, R. L. In *Inorganic Chemistry*, 4th ed.; HarperCollins: New York, 1993; p 292.
(50) Fallon, G. D.; Nichols, P. J.; West, B. O. *J. Chem. Soc., Dalton Trans.* **1986**, 2271−2276.
(51) Nguyen, D. H.; Hsu, H. F.; Munck, E.; Millar, M.; Koch, S. A. *J. Am. Chem. Soc.* **1996**, *118*, 8963.
(52) Baidya, N.; Olmstead, M.; Mascharak, P. K. *Inorg. Chem.* **1991**, *30*, 929−937.
(53) Baidya, N.; Olmstead, M. M.; Mascharak, P. K. *J. Am. Chem. Soc.* **1992**, *114*, 9666−9668.
(54) Swenson, D.; Baenziger, N. C.; Coucouvanis, D. *J. Am. Chem. Soc.* **1978**, *100*, 1932.
(55) Castro, R.; Garcia-Vazquez, J. A.; Romero, J.; Sousa, A.; Hiller, W.; Strahle, J. *Polyhedron* **1994**, *13*, 273−279.
(56) Corwin, D. T., Jr.; Koch, S. A. *Inorg. Chem.* **1988**, *27*, 493−496.